Sound propagation and damping in the vicinity of the smectic-*A*–hexatic-*B* phase transition of 4-propionyl-4′-*n*-heptanoyloxyazobenzene

D. Collin,[1] V. Reys,[1] J. L. Gallani,[1,*] L. G. Benguigui,[1,†] G. Poeti,[2] and P. Martinoty[1]
[1]*Laboratoire de Dynamique des Fluides Complexes, Unité Mixte de Recherche CNRS-ULP No. 7506, Université Louis Pasteur, 4 rue Blaise Pascal, 67070 Strasbourg Cedex, France*
[2]*Istituto Chimico della Università degli Studi di Camerino, Via S. Agostino 1, 62032 Camerino, Italy*
(Received 15 December 1997; revised manuscript received 7 April 1998)

Sound velocity and damping were measured in 4-propionyl-4′-*n*-heptanoyloxyazobenzene above its Sm-*A*–Hex-*B* phase transition. The measurements were taken at 1 MHz (velocity) and at 3, 9, 15, and 21 MHz (damping) as a function of the angle θ between the sound propagation direction and the normal to the smectic layers. The velocity presents a marked anomaly for $\theta=90°$, whereas a much smaller anomaly is observed for $\theta=0°$, indicating that the phase transition occurs essentially within the smectic layers. Analysis of these measurements allows the de Gennes elastic constants A, B, and C to be determined. Like the velocity, the damping presents significant pretransitional effects for $\theta=90°$, reminiscent of those generally observed in the vicinity of second-order or weakly first-order phase transitions. The damping also increases for $\theta=0°$ when $T\rightarrow T_{A\text{-Hex}}$, but the behavior observed does not resemble the usual critical behavior. It is shown that this pseudocritical behavior stems essentially from a contribution of the anharmonic effects. The anisotropy of the critical effects on velocity and damping can be explained by the theory elaborated by Andereck and Swift for the Sm-*A*–Sm-*C* transition and transposed to the Sm-*A*–Hex-*B* transition. Analysis of the velocity measurements indicates that the specific-heat exponent is of the order of 0.6. This value, which is far from that associated with the three-dimensional *XY* universality class -0.007 to which this transition should in principle belong, confirms the results obtained by calorimetry. The critical relaxation time is characterized by the dynamic exponent $z\nu\simeq 1$, which corresponds to conventional critical slowing down.
[S1063-651X(98)11107-8]

PACS number(s): 64.70.Md, 61.30.−v, 62.80.+f

I. INTRODUCTION

The notion of hexatic order was introduced in order to describe the fusion of a two-dimensional solid by proliferation of defects [1]. This description predicts the existence of a new state of matter, occurring between the crystalline solid and the isotropic liquid [2]. This intermediate phase, called hexatic for systems with hexagonal symmetry, is a state in which the positional order of the two-dimensional network has been lost but the orientational order of the crystallographic axes, known as the bond-orientational order, continues to exist. To be more precise, this phase possesses a short-range translational order and a quasi-long-range bond-orientational order. This latter is characterized by a local order parameter $\psi(r)=\langle e^{6i\theta(r)}\rangle$, where the brackets indicate a coarse-grain average and θ is the angle between the reference axis and a bond joining two neighboring molecules.

Birgeneau and Litster [3] have suggested that this description could be applied to some smectic phases of liquid crystals, provided that the quasi-long-range bond-orientational order is assumed to become a true long-range order. These predictions have proved to be correct, as smectic phases with a short-range positional order and a long-range bond-orientational order have indeed been observed [4]. These phases, called stacked hexatics, have their molecules perpendicular to the layers (Hex*B*), or inclined in relation to the normal to the layers (Hex*I*, Hex*F*, and Hex*L*). At the moment, these phases are the object of considerable attention, since they constitute excellent systems for studying the properties of the hexatic order [5].

The Sm-*A*–Hex-*B* transition is the simplest transition between an ordinary smectic phase and a stacked hexatic phase, since the molecules are perpendicular to the layers in both phases. The symmetry of the hexatic order parameter puts this transition in the 3D-*XY* universality class. The heat-capacity critical exponent $\overline{\alpha}$ should then be given as -0.007. Specific-heat experiments [5] carried out on a large number of compounds show, however, that $\overline{\alpha}$ has a value ($\overline{\alpha}\simeq 0.6$) which is totally incompatible with 3D-*XY* behavior. One proposed explanation for these large $\overline{\alpha}$ values is the proximity of a tricritical point [6,7]. However, the absence of variation of $\overline{\alpha}$ along the Sm-*A*–Hex-*B* transition line in binary mixtures seems to rule out this tricritical behavior [8]. Another possibility based on the high anisotropy of the transition has been suggested by Brock *et al.* [9]. The specific-heat exponent could be an apparent exponent associated with the fact that the system evolves from a two-dimensional type behavior far from the transition to a three-dimensional type behavior near the transition. Recently, Haga *et al.* [10] argued that the specific-heat behavior could arise from a coupling between the amplitude of the bond-orientational order

*Present address: Groupe des Matériaux Organiques, Institut de Physique et Chimie des Matériaux de Strasbourg, 23 rue du Loess, 67037 Strasbourg Cedex, France.
†Permanent address: Solid State Institute and Physics Department, Technion Israel Institute of Technology, Haifa 32000, Israel.

and the in-plane positional strain.

All the descriptions of the Sm-A–Hex-B transition assume that this transition occurs in a system of nonfluctuating layers, while in reality there are high-amplitude layer fluctuations that do not allow a long-range positional order to become established and totally alter the hydrodynamics of the smectic phases [11]. The influence of these fluctuations on the Sm-A–Hex-B transition has been investigated by Selinger [12], who has pointed out the existence of a frustration associated with layer curvature, which is geometrical in origin, and which introduces a coupling between the order parameter ψ and the displacement of the layers $u(\mathbf{r})$. This coupling can transform the transition into a first-order transition if the hexatic-rigidity constants are high enough, and could increase the value of the specific-heat exponent. The effects of this coupling on the dynamics of the transition have not, as yet, been investigated.

In contrast to the static features, very few studies have been devoted to the dynamics of the Sm-A–Hex-B transition, and this article presents an ultrasound study of this transition, carried out on 4-propionyl-4′-n-heptanoyloxyazobenzene (PHOAB). Some preliminary measurements were presented in Ref. [13].

Section II reviews the ultrasound theories presently available, by means of which our results will be described. The experimental techniques and specific problems associated with the study of this transition are presented in Secs. III and IV. The results obtained are presented in Sec. V, and then analyzed and discussed in Secs. VI and VII.

II. THEORETICAL BACKGROUND

A. Behavior in the Sm-A phase far from the smectic-A–hexatic-B phase transition: The Martin-Parodi-Pershan and Mazenko-Ramaswamy-Toner theories

The Martin-Parodi-Pershan (MPP) [14] theory predicts that sound damping shall, in the smectic-A phases, be written as

$$\frac{\alpha(\theta)}{f^2}=a(\theta), \tag{1}$$

where f is the frequency of the ultrasound wave, and $a(\theta)$ is a constant which is dependent on the angle θ between the normal to the layers (directed along the axis Oz) and the direction of sound propagation. This form is quite similar to that which is found in conventional liquids, the only difference being that term $a(\theta)$ is anisotropic. This term is a function of the five viscosity coefficients (η_i) that characterize the smectic-A phases and is written

$$a(\theta)=\frac{2\pi^2}{\rho V^3(\theta)}\left[(\eta_2+\eta_4)\sin^2\theta+\eta_1\cos^2\theta+(4\eta_3+2\eta_5-\eta_2-\eta_4-\eta_1)\cos^2\theta\,\sin^2\theta\right]. \tag{2}$$

η_1, η_4, and η_5 are volume viscosities, whereas η_2 and η_3 are shear viscosities; η_2 corresponds to a flow within the plane of the smectic layers and η_3 to the flow of one layer in relation to the other.

This theory also predicts that the velocity V of the sound is anisotropic, and is written

$$\rho V^2(\theta)=A-2C\,\cos^2\theta+B\,\cos^4\theta, \tag{3}$$

where ρ is the density of the medium and A, B, and C are the elastic constants associated with the elastic energy of the smectic-A phase, which is given by

$$F_{\mathrm{el}}=\int d^3r\left[\frac{A}{2}\left(\frac{\delta\rho}{\rho}\right)^2+\frac{B}{2}(\nabla_z u)^2+C\left(\frac{\delta\rho}{\rho}\right)(\nabla_z u)+\frac{K_1}{2}\left(\frac{\partial^2 u}{\partial x^2}+\frac{\partial^2 u}{\partial y^2}\right)^2\right]. \tag{4}$$

u is the displacement of the layers along the Oz axis and $\delta\rho$ represents the variation of density. Equation (4) shows that the rigidity constants A, B, and C are related respectively to density variation, layer compression, and the coupling between layer compression and density variation. Constant K_1 is linked to the undulation energy of the layers.

In order to take into account the anharmonic terms that are characteristic of lamellar systems, the MPP theory has been modified by Mazenko, Ramaswamy, and Toner (MRT) [15]. The main consequence of these terms, which are associated with the substantial fluctuations of the smectic layers, is to destroy the dynamic independence of the system's modes. More precisely, they are responsible for a nonlinear coupling between the velocity field and the undulation modes of the thermally excited layers. This coupling leads to a $1/f$-type divergence of the volume viscosities. One of the consequences of this divergence is the modification of low-frequency ultrasound absorption, which is written

$$\frac{\alpha}{f^2}(\theta)=a(\theta)+\frac{b(\theta)}{f}, \tag{5}$$

where $a(\theta)$ is the conventional absorption term [Eq. (2)] and $b(\theta)/f$ the anharmonic contribution. In the case of the lowest-order calculation, term $b(\theta)$ is given by

$$b(\theta)=\frac{2\pi k_B T}{128\rho^{-1/2}}\left(\frac{B}{AK_1}\right)^{3/2}\left(\cos^2\theta-\frac{C}{B}\right)^2, \tag{6}$$

where A, B, C, and K_1 are the constants already defined, k_B the Boltzmann constant, and T the absolute temperature. Equation (6) is valid if $A\gg B$, C or $B\simeq 2C$. Higher-order calculation of $b(\theta)$ gives a formula similar to Eq. (6), the only difference being that elastic constants A, B, and C are replaced by unknown coefficients $\tilde{A}$, $\tilde{B}$, and $\tilde{C}$.

For all the smectic-A phases studied up to now, $B>C$ and $C>0$. In this case, Eq. (6), giving $b(\theta)$, points to the existence of an angle θ_0, given by $\cos^2\theta_0=C/B$, for which $b(\theta_0)=0$. The existence of this ''magic angle'' has been observed in terephthal-bis-p-p'-butylaniline (TBBA) [11]. This magic angle disappears in the case of higher-order effects when $\tilde{C}>\tilde{B}$.

Unlike damping, the velocity of the sound is almost completely unaffected by anharmonic effects, since the elastic constants A, B, and C are only weakly renormalized (logarithmic behavior). In practice, then, Eq. (3) remains valid.

B. The influence of order-parameter fluctuations

1. Free energy

In order to study the influence of the order-parameter fluctuations on the transition, the free energy of the smectic-*A* phase, in the vicinity of the Sm-*A*–Hex-*B* transition, was assumed to be written as the sum of various contributions.

(a) A Landau-Ginzburg-type contribution associated with the order-parameter fluctuations, given by

$$F_\psi=\frac{1}{2}\int dV\left[a|\psi|^2+\tfrac{1}{2}b|\psi|^4+\frac{1}{2M_V}|\nabla_z\psi|^2+\frac{1}{2M_T}|\nabla_T\psi|^2\right]. \tag{7}$$

In this development, M_T and M_V are the main values of a mass tensor, which is assumed to be isotropic in the plane of the layers (M_V is the value along axis Oz, which gives the direction perpendicular to the layers; M_T is the layer-plane value.) Critical behavior at the transition is governed by coefficient $a(T)$, which is written

$$a(T)=a'(T-T_C), \tag{8}$$

where T_C is the transition temperature.

(b) The contribution resulting from the deformation of the smectic layers, as previously defined by Eq. (4).

(c) A kinetic-type contribution resulting from a shift in the centers of mass,

$$F_V=\frac{1}{2}\int d^3r|\mathbf{V}|^2. \tag{9}$$

(d) Two final contributions, one coupling the order parameter with density variations, and the other with the layer-spacing gradients. These two contributions are given, respectively, by

$$F_{\psi\rho}=\frac{1}{2}\gamma_\rho\int d^3r\left(\frac{\delta\rho}{\rho}\right)|\psi|^2, \tag{10}$$

$$F_{\psi u}=\frac{1}{2}\gamma_u\int d^3r(\nabla_z u)|\psi|^2, \tag{11}$$

where γ_ρ and γ_u are phenomenological constants, to be determined experimentally.

The free energy of the smectic-*A* phase, in the vicinity of the Sm-*A*–Hex-*B* transition, is therefore written as

$$F=F_\psi+F_{\rm el}+F_v+F_{\psi\rho}+F_{\psi u}. \tag{12}$$

This form of free energy is identical to that used by Andereck and Swift to study the behavior of ultrasound velocity and damping in the vicinity of the Sm-*A*–Sm-*C* transition [16]. This formal analogy enables us to transpose the results of their calculations on to the Sm*A*-Hex*B* transition. These calculations concern the smectic-*A* phase only.

2. Modification of the elastic constants and the ultrasound velocity

Andereck and Swift's calculations were made within the framework of a mean-field-type theory, based on the existence of a quadratic coupling between the sound wave and the order parameter. The calculations show that the compound's elastic constants A, B, and C are modified by fluctuations of the order parameter, and are written

$$\begin{aligned}A&=A_{\rm reg}-\gamma_\rho^2 I_2,\\ B&=B_{\rm reg}-\gamma_u^2 I_2,\\ C&=C_{\rm reg}-\gamma_u\gamma_\rho I_2.\end{aligned} \tag{13}$$

Index ''reg'' indicates the value the elastic constants would have in the absence of any fluctuations; I_2 is a temperature- and frequency-dependent function, given by

$$I_2=\frac{4k_BT}{(\gamma_0)^2}\int\frac{d^3q}{(2\pi)^3}\frac{1}{[\omega^2+4\Gamma^2(\mathbf{q})]}, \tag{14}$$

where $\Gamma(\mathbf{q})$ represents the relaxation frequency of a fluctuation of the order parameter, with a wave vector $\mathbf{q}$, and γ_0 the viscosity associated with this relaxation frequency. $\Gamma(\mathbf{q})$ is given by

$$\Gamma(\mathbf{q})=\frac{1}{\gamma_0}\left(a+\frac{q_\perp^2}{2M_\perp}+\frac{q_z^2}{2M_z}\right). \tag{15}$$

Modification of the elastic constants implies a modification in the velocity, this latter being linked to the elastic constants by formula (3). Replacing A, B, and C with their modified values, $\rho V^2(\theta)$ can be rewritten as

$$\rho V^2(\theta)=\rho V_{\rm reg}^2(\theta)-\Delta[\rho V^2(\theta)], \tag{16}$$

where

$$\rho V_{\rm reg}^2(\theta)=A_{\rm reg}-2C_{\rm reg}\cos^2\theta+B_{\rm reg}\cos^4\theta \tag{17}$$

is the normal part of the velocity, and where

$$\Delta[\rho V^2(\theta)]=(\gamma_\rho-\gamma_u\cos^2\theta)^2 I_2 \tag{18}$$

is the critical part associated with the order-parameter fluctuations.

$V_{\rm reg}$ is the value that would be assumed by the velocity if the phase transition did not exist. From the acoustic point of view, this corresponds to infinite frequency, since, at this frequency, the system cannot follow ultrasound disturbance; $\rho V_{\rm reg}^2(\theta)$ therefore equals $\rho V^2(\theta,\infty)$ and Eq. (16) can be rewritten as

$$\rho V^2(\theta,\omega)=\rho V^2(\theta,\infty)-(\gamma_\rho-\gamma_u\cos^2\theta)^2 I_2. \tag{19}$$

This equation shows that velocity $V(\theta,\omega)$ decreases in the vicinity of the Sm-*A*–Hex-*B* transition, and that this decrease can be more-or-less important, according to the angle θ considered. For example, when $\gamma_\rho>\gamma_u$, the decrease associated with $V(90°)$ must be much greater than that associated with $V(0°)$.

3. Modification of viscosity coefficients and ultrasound damping

Fluctuations of the order parameter affect not only the compound's elastic constants, but also volume viscosities η_1, η_4, and η_5, which are written

$$\eta_1=(\eta_1)_{\mathrm{reg}}+(\gamma_\rho-\gamma_u)^2 I_1,$$
$$\eta_4=(\eta_4)_{\mathrm{reg}}+\gamma_\rho^2 I_1, \tag{20}$$
$$\eta_5=(\eta_5)_{\mathrm{reg}}+\gamma_\rho(\gamma_\rho-\gamma_u) I_1.$$

Index ''reg'' indicates the value the viscosities would have in the absence of any fluctuations; I_1 is given by

$$I_1=\frac{2k_BT}{\gamma_0}\int\frac{d^3q}{(2\pi)^3}\frac{\chi(\mathbf{q})}{[\omega^2+4\Gamma^2(\mathbf{q})]}, \tag{21}$$

where

$$\chi(\mathbf{q})=\frac{1}{\gamma_0\Gamma(\mathbf{q})}. \tag{22}$$

Since the volume viscosities are modified, the same will apply to ultrasound damping. In the cases of angles $\theta=0°$ and $\theta=90°$, the critical part of the damping is written

$$\frac{\Delta\alpha(0°)}{f^2}=\frac{\pi^2}{\rho V^3(0°)}(\gamma_\rho-\gamma_u)^2 I_1, \tag{23}$$

$$\frac{\Delta\alpha(90°)}{f^2}=\frac{\pi^2}{\rho V^3(90°)}\gamma_\rho^2 I_1. \tag{24}$$

These two formulas show that critical damping can be anisotropic, the rate of anisotropy depending on the values of γ_u and γ_ρ. More especially, if γ_ρ is greater than γ_u, the critical effect for $\theta=90°$ must be greater than that for $\theta=0°$.

4. Behavior of velocity and damping in the hydrodynamic regime ($\omega\tau\ll 1$)

The hydrodynamic behavior of the critical parts of the velocity and damping is obtained by taking the zero-frequency limit of the functions I_1 and I_2, and is given by

$$\Delta[\rho V^2(\theta)]=Pf(\theta)(T-T_C)^{-\bar{\alpha}}, \tag{25}$$

$$\frac{\Delta\alpha(\theta)}{f^2}=Qf(\theta)(T-T_C)^{-x}. \tag{26}$$

P and Q are constants which are function of M_T, M_V, and γ_0. The function $f(\theta)$ is given by

$$f(\theta)=\left(1-\frac{\gamma_u}{\gamma_\rho}\cos^2\theta\right)^2 \tag{27}$$

and the exponent x by

$$x=\bar{\alpha}+z\nu. \tag{28}$$

$\bar{\alpha}$ is the specific-heat exponent and $z\nu$ the exponent associated with the critical relaxation time τ which is defined by [16]

$$\tau\sim\xi^z\sim(T-T_C)^{-z\nu}, \tag{29}$$

where ξ is the correlation length.

Equation (25) shows that the critical behavior of the velocity reflects that of the specific heat.

Finally, it should be noted that the amplitude of the critical damping is linked to that of the velocity dispersion $\Delta[\rho V^2(\theta)]=\rho V^2(\theta,\infty)-\rho V^2(\theta,0)$ by the relationship

$$\lim_{f\to 0}\frac{\Delta\alpha(\theta)}{f^2}=\pi^2\frac{\Delta[\rho V^2(\theta)]}{4\rho V^3(\theta)}\tau(q=0), \tag{30}$$

where $\tau(q=0)$ is the relaxation time of the longest-wavelength mode.

III. EXPERIMENTAL TECHNIQUES

The experiments were carried out by means of resonance and pulse techniques, with 3-MHz quartz crystals. The pulse device allowed the damping measurements to be taken at 3, 9, 15, and 21 MHz, and the resonance technique was used for its capacity to measure simultaneously the velocity and damping in the megahertz range. By means of a simple switch, it was possible to take pulse and resonance measurements on the same cell. This enabled a significant comparison to be made between the two types of measurements thus taken on the same sample.

The resonator consists of two identical transducers (X-cut quartz) with the liquid to be studied in between. One of the transducers is excited by a tunable-frequency sine voltage. This generates a compressional wave which is propagated in the liquid and travels forward and backward between the transducers. A standing-wave sound field occurs in the cell each time the interquartz length is matched by a whole multiple of the half wavelength (i.e., resonance is present). The resonance signal is detected by the receiver quartz, then amplified and displayed on an oscilloscope. The characteristics of resonance peaks (width at -3 dB, central frequency) enable the velocity V and the ultrasonic damping per wavelength $\alpha\lambda$, to be determined according to the following formulas:

$$V=2l\delta f, \tag{31}$$

$$\alpha\lambda=\frac{\pi\Delta f}{f}. \tag{32}$$

In these formulas, Δf is the width of a peak at -3 dB and f its central frequency; δf is the gap between two adjacent peaks and l the cell length (interquartz distance).

For pulse measurements, the continuous signal supplied by a rf generator is gated by rectangular pulses in a diode modulator. The pulses thus obtained are amplified and then applied to the transmitter quartz in the cell. Measuring consists in reading the amplitude of the various echoes at the frequency concerned.

All the cells used were cylindrical in form with interquartz distances ranging from 3.22 to 3.92 mm. The diameter of the sample ($\varnothing=38$ mm) was chosen to be larger than that of the ultrasonic beam ($\varnothing=25$ mm) in order to minimize possible parasitic effects due to the side walls.

The smectic samples were oriented by heating the compound in its isotropic phase and subsequently cooling it gently in the presence of a 10-kG magnetic field delivered by an electromagnet. The orientation is characterized by the angle θ between the direction of the magnetic field and the direction of sound propagation. The study was made with orientations $\theta = 0°$, 45°, and 90°.

The cells were never completely filled, and were placed between the poles of the electromagnet in such a way that the smectic planes of the sample were vertical. These precautions, which allow the sample to expand, reduce the layer-undulation instabilities that appear when the sample is under mechanical or thermal stress. A detailed description of the experimental technique and the cell can be found in Ref. [11].

IV. SPECIFIC PROBLEMS ASSOCIATED WITH THE SMECTIC-*A*–HEXATIC-*B* TRANSITION IN PHOAB

A. The compound

This study of the Sm-*A*–Hex-*B* transition was carried out on 4-propionyl-4′-*n*-heptanoyloxyazobenzene (PHOAB), the formula of which is reproduced below:

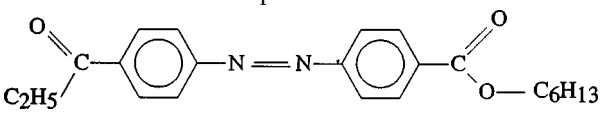

This is one of the few compounds which, in addition to smectic-*A* and hexatic-*B* phases, presents the nematic phase required in order to obtain smectic samples which are volume orientated by a magnetic field. Its hexatic phase was identified by means of miscibility [17] and x-ray [18] studies. Dilatometric and calorimetric studies [19] of the Sm-*A*–Hex-*B* transition have shown that this is a first-order transition.

B. The first-order nature of the Sm-*A*–Hex-*B* transition and its consequences

In the case of first-order transitions, there is a temperature zone, in the vicinity of the transition temperature itself, where both phases coexist. The width of this zone can be experimentally determined by measuring temperatures T_{C1} and T_{C2}, associated respectively with its appearance and disappearance as temperature falls. The thermodynamic transition is situated in between T_{C1} and T_{C2}. The coexistence zone is generally a function of the concentration of impurities in the sample, which has the effect of increasing its width and reducing the temperature T_{C1} at which it occurs. Although this coexistence zone has been observed in some cases by using ultrasound resonance techniques [20], it has not been possible to detect it in this study as a result of the excessively high value of damping, leading to significant broadening or disappearance of the resonance peaks. Optical microscopy [21] and dilatometry [19] experiments have suggested that the coexistence zone associated with the Sm-*A*–Hex-*B* transition of PHOAB stretches over a non-negligible range of temperatures, of the order of 0.2 °C for the purest compounds.

These coexistence phenomena do not exist for second-order transitions and there is therefore only a single transition temperature T_C. These transitions are characterized acoustically by a damping peak and a velocity dip which, in the hydrodynamic regime, appear at T_C.

The measurements taken on PHOAB also reveal the existence of a damping peak and, for some orientations, a velocity dip. These anomalies occur at a temperature that we have called T_{peak}, which is not well defined, as it is probably situated within the coexistence zone. That is why our measurements are shown with respect to the transition temperature $T_{N\text{-}I}$. In spite of the fact that the *N*-*I* transition is also a first-order transition, its coexistence zone is narrow (<0.1 °C), with the result that $T_{N\text{-}I}$ can be defined as the temperature associated with the damping peak. $T_{N\text{-}I}$ is therefore known to within ± 0.05 °C.

C. Precautions taken in order to avoid sample deterioration

PHOAB is a compound that deteriorates very easily. This deterioration is evidenced by a substantial decrease in the transition temperatures (*N*-*I*, *N*–Sm-*A*, and Sm-*A*–Hex-*B*), and also by a broadening of the coexistence zone of the phases concerned. Using PHOAB therefore requires the elaboration of an experimental method enabling the samples to be kept at a high degree of purity throughout the whole experimental process. We used the method developed in our laboratory for ultrasound study of TBBA [11], which consists in taking measurements in an inert atmosphere, any trace of air dissolved in the sample having been eliminated. This is why the sample was degassed inside the cell itself, and the measurements taken in an inert nitrogen atmosphere. In spite of these precautions, slight deterioration of the compound could not be avoided, which was not so in the case of TBBA.

D. Determination of velocity and damping

In Sec. III, we have seen that in order to determine the velocity, it is necessary to know interquartz distance l, and this can be obtained using a reference liquid of known velocity. This method enables l and therefore V, to be determined, to within 0.5%, which leads to an uncertainty of the order of ± 5 m/s for a velocity of the order of 1000 m/s. This uncertainty, which affects each of the velocity measurements corresponding to a given angle θ, is too great to allow accurate determination of elastic constants B and C, which are associated with the low anisotropy of the velocity.

In order to determine these constants accurately, the following method was used. For each angle θ, we measured the variation in velocity as a function of temperature, from the isotropic phase through to the temperature at the end of the experiment. The resulting curves were plotted as a function of $T\text{-}T_{N\text{-}I}$, then superimposed on each other in the isotropic phase. This renormalization of the various curves is justified by the fact that the velocity measurements in the isotropic phase are independent of angle θ. Uncertainty concerning the velocity measurements stems essentially from this renormalization, and is of the order of ± 20 cm/s, for the measurements presented in this paper.

Damping in the Sm-*A* phase was determined by the pulse method, measuring the amplitude of the first echo as a function of temperature in relation to a reference value determined in the isotropic phase. This normalization was performed at 11 °C from the *N*-*I* transition temperature, where

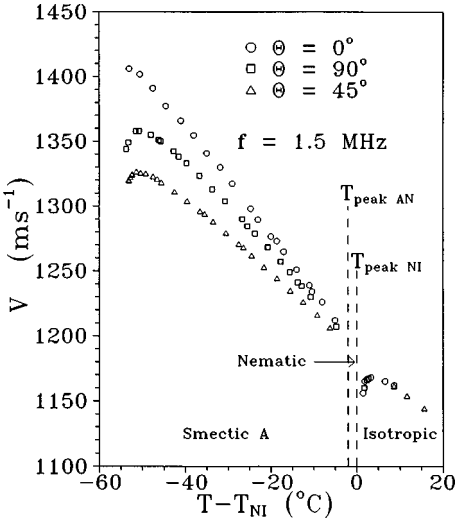

FIG. 1. Variation of velocity as a function of temperature for $\theta=0°$, 45°, and 90°. θ is the angle between the normal to the smectic layers and the direction of sound propagation. As the hexatic phase is approached, velocity presents pretransitional effects which are large for $\theta=90°$ and practically nonexistent for $\theta=0°$. The disappearance of the resonance peak precludes any velocity measurements for temperatures below $T_{peak}+1.5\,°C$. T_{peak} is the temperature at which 3-MHz damping reaches its maximum value.

the α/f^2 ratio is frequency independent within the limits of experimental accuracy, and is $\simeq 1000\times10^{-17}$ cm^2 s^{-1}.

At temperatures very far from the Sm-A–Hex-B transition, damping is usually sufficiently weak for several echos to be observable, and can therefore be measured directly and compared to the value previously obtained. The results obtained show that these two methods produce comparable results.

One final point concerns the reproducibility of the measurements. The various experiments carried out have shown that velocity measurements taken at 1.5 MHz are reproducible whatever the angle concerned ($\theta=0°$, 45°, and 90°). The same observation holds for the damping measurements taken at 3, 9, 15, and 21 MHz for $\theta=0°$ and 90°. However, the damping measurements for $\theta=45°$ are not reproducible, the damping value varying by a factor as high as 2 from one experiment to the next. In our opinion, this nonreproducibility is linked to poor orientation of the smectic planes. These 45° damping measurements will not be taken into account.

V. RESULTS

Figure 1 gives the thermal variation of velocity at $f\simeq1.5$ MHz for the three orientations defined by $\theta=0°$, 45°, and 90°. For $\theta=45°$ and 90°, it was not possible to measure the velocity for temperatures below $T_{peak}+1.5\,°C$, owing to a very substantial increase in damping, which leads to the disappearance of the resonance peaks. On the other hand, these measurements could be made for $\theta=0°$, since there is less damping at that orientation, but they present a considerable uncertainty, since the resonance peaks are very wide. These measurements, which can also be affected by the coexistence zone, are not shown in Fig. 1.

Examination of Fig. 1 reveals the existence of pretransitional effects (a decrease in velocity), the amplitude of which is a function of angle θ. These effects are great for $\theta=90°$ (propagation in the plane of the layers), and practically nonexistent for $\theta=0°$ (propagation perpendicular to the layers). This marked difference in behavior indicates that the transition takes place essentially within the smectic layers.

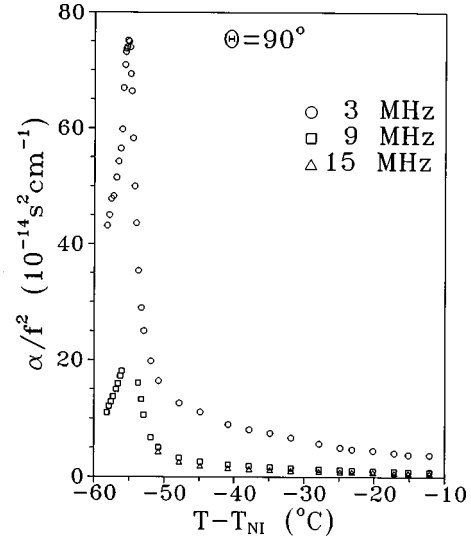

FIG. 2. Variation of α/f^2 at 3, 9, and 15 MHz as a function of temperature for $\theta=90°$. The results reveal the existence of considerable pretransitional effects on each side of the transition. 9- and 15-MHz damping is too great to be measured near the transition.

Like velocity, damping also presents important pretransitional effects for $\theta=90°$ (see Fig. 2), which are similar to those generally observed near a second-order or a weakly first-order transition. Very high damping values preclude any measurements in the vicinity of the transition for the 9- and 15-MHz frequencies.

For $\theta=0°$ (Fig. 3), damping also increases as the transition is approached, but the amplitude of the effect is much smaller than for $\theta=90°$ and does not resemble the fast in-

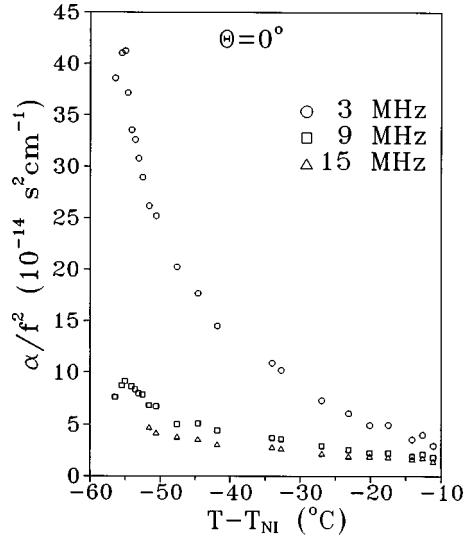

FIG. 3. Variation of α/f^2 at 3, 9, and 15 MHz as a function of temperature for $\theta=0°$. The behavior of α/f^2 is very different from that observed for $\theta=90°$ (Fig. 2), and reflects the influence of anharmonic effects (see text).

crease associated with the usual critical behavior. This quite unexpected pseudocritical behavior shall be seen below to come from anharmonic effects. The relative position of the 3- and 9-MHz damping peaks is not known with accuracy, owing to the considerable uncertainty over the measurements in the vicinity of the transition. As for $\theta=90°$, the very high damping value precludes any measurements at 15 MHz near the transition.

VI. ANALYSIS OF THE VELOCITY MEASUREMENTS AND DETERMINATION OF THE ELASTIC CONSTANTS *A*, *B*, AND *C*

A. Analysis of the velocity measurements

Velocity measurements were analyzed with the formula

$$V^2(\theta)=V^2_{\rm reg}(\theta)-\Delta V^2(\theta), \tag{33}$$

in which $V^2_{\rm reg}(\theta)$ represents the regular term and $\Delta V^2(\theta)$ the critical one. The latter is given by Eq. (25), in which we have assumed $\rho=1$ g cm^{-3}. Since the behavior of $\Delta V^2(\theta)$ reflects that of the specific heat, we have incorporated into Eq. (25) the constant $q_{\rm crit}$, in order to obtain an expression similar to that used for the specific-heat analyses [22]. In these conditions, $\Delta V^2(\theta)$ is written as

$$\Delta V^2(\theta)=f(\theta)[P(T-T^*_C)^{-\overline{\alpha}}+q_{\rm crit}], \tag{34}$$

where T^*_C represents the virtual transition temperature at which the Sm-*A*–Hex-*B* transition would occur if it were of the second order and $f(\theta)$ is given by Eq. (27). The difference $T-T^*_C$ is linked to the difference $T-T^*_{N\text{-}I}$ by the relationship

$$T-T^*_C=(T-T_{N\text{-}I})+(T_{N\text{-}I}-T^*_C). \tag{35}$$

Formula (34) assumes that the velocity measurements correspond to the hydrodynamic regime ($\omega\tau\ll 1$), and are therefore frequency independent. This assumption will be justified later, when the damping measurements are analyzed. If $\overline{\alpha}$ is positive, $\Delta V^2(\theta)$ diverges, and Eq. (33) shows that $V^2(\theta)$ becomes negative at the transition, which is not physically correct. In principle, one should consider the critical behavior of the bulk compliance. However, Eq. (33) is valid as long as $\Delta V^2/V^2_{\rm reg}\ll 1$, which is the hypothesis on which the theory is based. In the present case, the maximum value of $\Delta V^2/V^2_{\rm reg}\simeq 0.067$.

We have assumed that variation of the regular term is linear with temperature, as shown by the behavior of $V^2(\theta)$ observed far from the Sm-*A*–Hex-*B* transition. This linear behavior, which stems from the fact that the *N*–Sm-*A* transition is strongly first order, can be written as

$$V^2_{\rm reg}(\theta)=S(\theta)(T-T_{N\text{-}I})+q_{\rm reg}(\theta). \tag{36}$$

Since the behavior of velocity in the vicinity of the Sm-*A*–Hex-*B* transition is characterized by very anisotropic critical effects, the $V^2(\theta)$ measurements were analyzed as follows. We first considered the measurements associated with $\theta=90°$ and 45°, which have marked critical behavior. Then we used the parameters obtained from these analyses to calculate the behavior for $\theta=0°$ and verify that it is compatible with the observed behavior, which has a very small critical effect.

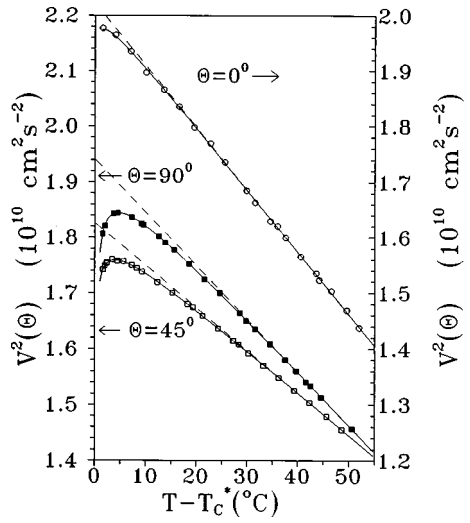

FIG. 4. Analysis of $V^2(\theta)$ measurements. The dashed lines correspond to the velocity values that would be found if the Sm-A–Hex-B transition did not exist. The solid lines represent fit 1 of Table I made with Eq. (34).

The behaviors of $V^2(90°)$ and $V^2(45°)$ show variations which are linear with temperature for temperatures higher than $T=T_{N\text{-}I}-25$ °C for $\theta=45°$, and $T=T_{N\text{-}I}-20$ °C for $\theta=90°$. The fit of Eq. (36) to the experimental results gives for $\theta=90°$

$$S(90°)=[-9.6\pm 0.1]\times 10^7 \ \ {\rm cm^2\ s^{-2}\ K^{-1}},$$

$$q_{\rm reg}(90°)=[1.401\pm 0.001]\times 10^{10} \ \ {\rm cm^2\ s^{-2}}$$

and for $\theta=45°$

$$S(45°)=[-7.64\pm 0.06]\times 10^7 \ \ {\rm cm^2\ s^{-2}\ K^{-1}},$$

$$q_{\rm reg}(45°)=[1.404\pm 0.001]\times 10^{10} \ \ {\rm cm^2\ s^{-2}}.$$

Figure 4 shows that these fits, which are shown by the dashed lines, give a good description of the data far from the Sm-*A*–Hex-*B* transition.

With the regular terms $V^2_{\rm reg}(90°)$ and $V^2_{\rm reg}(45°)$ known, the critical terms $\Delta V^2(90°)$ and $\Delta V^2(45°)$ can now be determined, and analyzed using Eq. (34). In order to take into account the fact that the thermal behavior of $\Delta V^2(90°)$ and $\Delta V^2(45°)$ must be described by the same law, we adjusted Eq. (34) to the whole set of data obtained for $\theta=45°$ and $\theta=90°$. The adjustable parameters are P, $q_{\rm crit}$, $\overline{\alpha}$, γ_u/γ_ρ, and T^*_C. In order to take into account the fact that the measurements for each orientation were taken on a different sample, T^*_C was assumed to be an adjustable parameter, which may be different for $\theta=45°$ and $\theta=90°$. The fit was made using measurements between $T=T_{N\text{-}I}-53.8$ °C and $T=T_{N\text{-}I}-25$ °C. This interval takes into account the data that are the closest to the transition and excludes those that allowed us to estimate the terms $V^2_{\rm reg}(90°)$ and $V^2_{\rm reg}(45°)$.

This temperature range corresponds to fit 1 in Table I. For each angle θ, the γ_u/γ_ρ, $T^*_C(90°)$, and $T^*_C(45°)$ values

TABLE I. Values of the adjustable parameters obtained from least-squares fits of $\Delta V^2(90°)$ and $\Delta V^2(45°)$ data with Eq. (34). $T_{\min}$ is equal to $T_{N\text{-}I}-53.8$ °C for $\theta=90°$, and $T_{N\text{-}I}-53.2$ °C for $\theta=45°$. The values of T_C^* for $\theta=90°$ and 45° are not the same, since the measurements were taken on different samples. Standard deviations are given for each least-squares parameter value.

Fit	Temperature range (°C)	T_c ($\theta=90°$)(°C)	T_c ($\theta=45°$)(°C)	P ($10^{10}\times$cm^2 s^{-2} K^{-1})	q_{crit} ($10^{10}\times$cm^2 s^{-2})	$\overline{\alpha}$	γ_u/γ_ρ
1	$[T_{\min},T_{N\text{-}I}-25]$	$[T_{N\text{-}I}-55.3\pm0.2]$	$[T_{N\text{-}I}-54.8\pm0.2]$	0.18 ± 0.01	-0.020 ± 0.003	0.61 ± 0.06	0.49 ± 0.02
2	$[T_{\min},T_{N\text{-}I}-35]$	$[T_{N\text{-}I}-55.3\pm0.3]$	$[T_{N\text{-}I}-54.8\pm0.3]$	0.18 ± 0.02	-0.020 ± 0.008	0.6 ± 0.1	0.49 ± 0.02
3	$[T_{N\text{-}I}-50.5,T_{N\text{-}I}-25]$	$[T_{N\text{-}I}-55.6\pm1.6]$	$[T_{N\text{-}I}-54.3\pm1.5]$	0.20 ± 0.10	-0.019 ± 0.009	0.6 ± 0.2	0.54 ± 0.06

given by this table, enable the behavior of the $\Delta V^2(\theta)/f(\theta)$ ratio versus $T\text{-}T_C^*$ to be determined. According Eq. (27), we have $f(90°)=1$ and $f(45°)=[1-\frac{1}{2}(\gamma_u/\gamma_\rho)]^2$. Both the behaviors obtained are given in Fig. 5. They show that all the data fit onto a single curve, which indicates that the critical effects are identical to within the anisotropy factor. The solid line shows the fit obtained with the values of P, q_{crit}, $\overline{\alpha}$, and γ_u/γ_ρ given by fit 1 in Table I. Several temperature intervals were used in order to test the stability of the fit. The parameters associated with each of the analyses are included in Table I.

Fit 2 excludes the data the farthest from the transition and shows that a 10 °C reduction in the temperature interval does not modify the parameters relating to fit 1. Fit 3 excludes the data the closest to the transition. Although the observed critical effects are very greatly reduced, this fit gives parameters close to those of fit 1. There is greater uncertainty with these parameters, however, since the fit does not take into account all the experimental data associated with the critical effects. These two analyses therefore indicate that the parameters deduced from fit 1 can be taken to be significant. In particular, the value of the γ_u/γ_ρ ratio is of the order of 0.5.

Let us now consider the results obtained for $\theta=0°$, which shows no marked critical effect. In order to analyze these results, we first of all determined the regular contribution $V^2_{\text{reg}}(0°)$. This is given by the linear behavior of $V^2(0°)$ with temperature, which is shown as a dashed line in Fig. 4. The fit of Eq. (36) to the experimental plot associated with temperatures between $T_{N\text{-}I}-30$ °C and $T_{N\text{-}I}-5$ °C gives the following resulting parameters: $S(0°)=[-1.122\pm0.005]\times10^8$ cm^2 s^{-2} K^{-1} and $q_{\text{reg}}(0°)=[1.403\pm0.001]\times10^{10}$ cm^2 s^{-2}. Since the regular contribution is known, it is now possible to determine the critical one $\Delta V^2(0°)$. Since this latter is very weak, we have, in Eq. (34), imposed the values of $\overline{\alpha}$, γ_u/γ_ρ, P, and q_{crit} deduced from fit 1 of Table I, keeping T_C^* as the only adjustable parameter. The fit obtained with $T_C^*=T_{N\text{-}I}-(55.1\pm0.2)$ °C is given as the solid line in Fig. 4, and shows that the decrease expected for $V^2(0°)$ must only occur for temperatures below $T-T_C^*=1.5$ °C. This slight decrease in velocity can hardly be observed experimentally, owing to the wide dispersion of measurements in this temperature range.

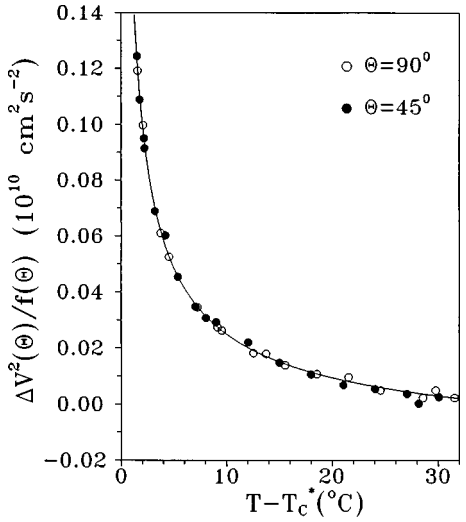

FIG. 5. Critical behavior of the square of the velocity divided by the anisotropy factor. The solid line represents fit 1 of Table I made with Eq. (34).

All the experimental results can thus be described satisfactorily using the model applied. The $\gamma_\rho>\gamma_u$ inequality reflects the fact that the critical effects are very anisotropic, and originate essentially within the smectic layers. Since the previous analyses have been performed without correction-to-scaling terms [23], the critical exponent $\overline{\alpha}$ ought to be considered as an effective exponent that describes the range of data fitted and does not necessarily reflect the asymptotic behavior.

The value of exponent $\overline{\alpha}$ ($\overline{\alpha}\simeq0.6$) agrees with that determined by the specific-heat measurements taken on other compounds with a Sm-A–Hex-B transition [5]. Specific-heat measurements have also been made on PHOAB by Huang, Nounesis, and Guillon [24]. These authors have emphasized that a power law could not account for their measurements, but this fit was done without taking into account the first-order nature of the transition. These measurements can, in fact, be described with a power law, provided one ignores the data closest to the transition, and a rough analysis of these measurements gives an $\overline{\alpha}$ value similar to those determined for the other Sm-A–Hex-B transitions.

B. Determination of elastic constants A,B,C

These constants can be calculated by Eq. (3), which gives the angular variation of velocity. As before, it was assumed that $\rho=1$ g cm^{-3}. The three constants and their thermal variation have been calculated using the fits determined in the previous paragraph, and are shown as solid lines in Fig. 6. The values (A_{reg}, B_{reg}, and C_{reg}), which these constants would have if the phase transition did not exist, are also shown in Fig. 6, as dashed lines. Examination of this figure shows that A decreases strongly when $T\rightarrow T_C^*$, this decrease is less marked for C, and hardly visible for B. This more-or-less marked decrease of the elastic constants once again reflects the fact that $\gamma_\rho>\gamma_u$ [cf. Eq. (13)]. The opposite result was obtained for the Sm-A–Sm-C transition [25], since

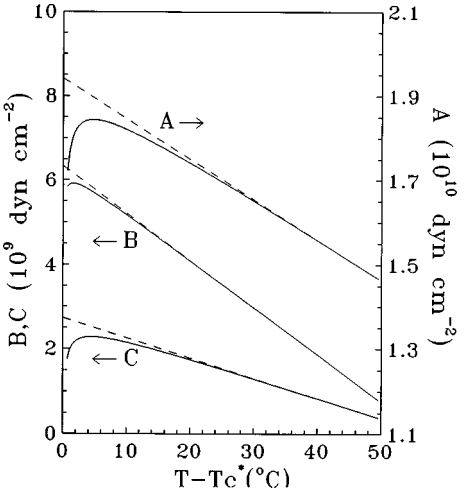

FIG. 6. Variation of elastic constants A, B, and C vs $T-T_C^*$. These constants are deduced from Eq. (3) using the velocity-data analysis from Fig. 4. The dashed lines correspond to the values that would be found for these constants if the Sm-A–Hex-B transition did not exist.

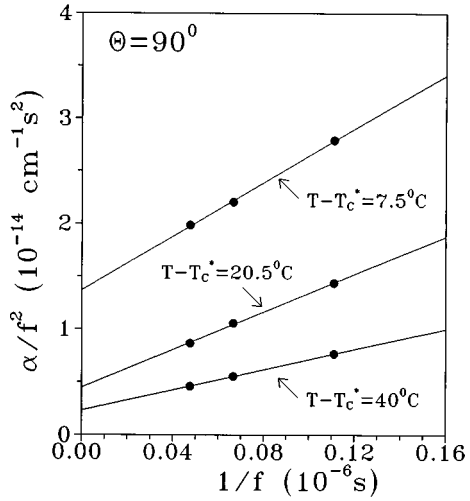

FIG. 7. Variation of α/f^2 as a function of $1/f$. The linear behavior is consistent with Eq. (37).

B and A were the constants that were respectively the most affected and the least affected by the transition. It should be noted that $B \simeq 2C$, which allows us to use Eq. (6) to calculate the anharmonic contribution.

VII. ANALYSIS OF THE DAMPING MEASUREMENTS

In order to analyze these measurements, we have assumed that total damping is the sum of three contributions:

(1) A critical contribution, assumed to be frequency independent (hydrodynamic regime), which will be confirmed by the results of data analysis—this contribution is given by Eq. (26).

(2) A conventional contribution, the MPP contribution [14], which is given by Eq. (1)—this contribution, which is due to viscosity, will be assumed constant for each orientation throughout the whole temperature range studied.

(3) An anharmonic contribution, typical of the smectic phases, which is given by Eq. (6).

Our measurements will therefore be analyzed using the following equation:

$$\left(\frac{\alpha(\theta)}{f^2}\right) = Qf(\theta)(T-T_C^*)^{-x} + \frac{2\pi k_B T}{128\rho^{-1/2}}\frac{1}{f}\left(\frac{B}{AK_1}\right)^{3/2}\left(\cos^2\theta - \frac{C}{B}\right)^2 + a(\theta). \tag{37}$$

Equation (37) will be seen below to give a good account of our experimental 9-, 15-, and 21-MHz results, but not to apply to those obtained at 3 MHz. This is why our presentation of the results will separate those obtained at 9, 15, and 21 MHz from those at 3 MHz.

A. Analysis of the 9-, 15-, and 21-MHz results

1. Analysis of the anharmonic effects

We shall first begin by analyzing the α/f^2 measurements obtained at each temperature as a function of frequency. Figure 7, associated with the $\theta = 90°$ orientation, shows linear variation of α/f^2 with $1/f$. The results for $\theta = 0°$ (not shown here) show similar behavior. According to formula (37), the slope of these straight lines gives the anharmonic contribution, and the ordinate at the origin gives the background term associated with the critical term and the conventional viscosity term. This same formula shows that the B/C ratio can be deduced from the ratio of the slopes obtained for $\theta = 0°$ and $\theta = 90°$. Figure 8 shows that the B/C ratio thus determined is, to within 10%, equal to that deduced from the velocity measurements, which constitutes an argument in favor of the lowest-order development of the theory. Using values of A, B, and C from the velocity measurements enables the behavior of K_1 to be determined. This is also shown in Fig. 8,

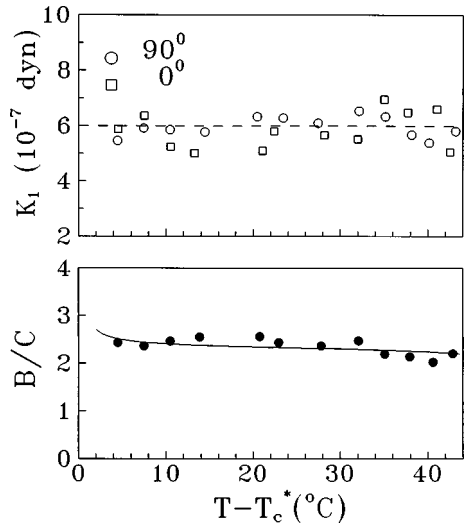

FIG. 8. Lower panel: behavior of the B/C ratio as a function of temperature. The points are deduced from the 0°- and 90°-damping measurements by using Eq. (37). This behavior of B/C is in agreement with that (in solid line) deduced from velocity measurements (Fig. 6). Upper panel: behavior of K_1 as a function of temperature. K_1 is deduced from the $1/f$ behavior of α/f^2 by using Eq. (37) and the values of the elastic constants A, B, and C. K_1 is temperature independent and has a mean value (shown by the dashed line) which is near those determined for other compounds (see text).

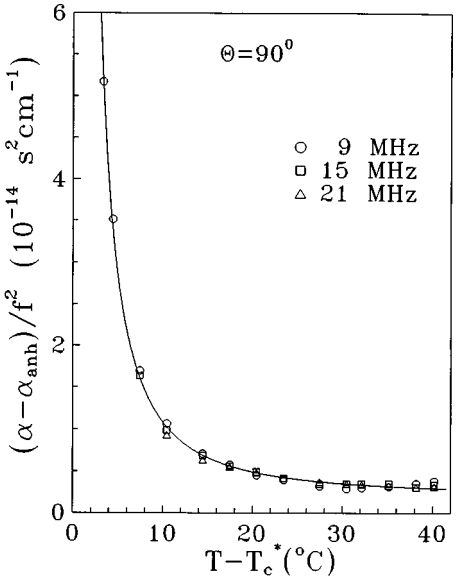

FIG. 9. Behavior of α/f^2 obtained for $\theta=90°$ after subtracting the anharmonic effects. The fact that α/f^2 is frequency independent indicates that the measurements are in the hydrodynamic regime. The solid line represents the fit to Eq. (38).

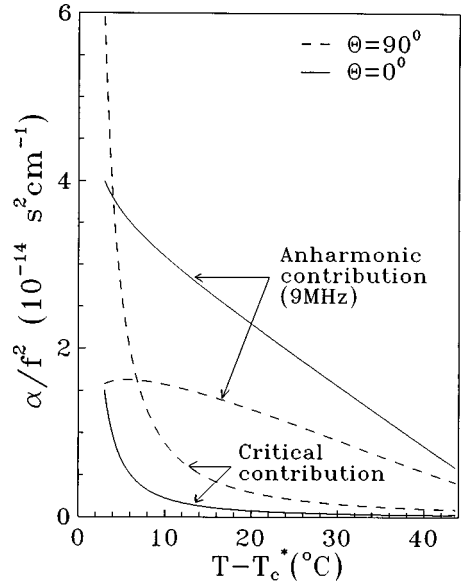

FIG. 10. Comparison of critical and anharmonic contributions for $\theta=90°$ and 0°. The importance of the anharmonic contribution for $\theta=0°$ explains the pseudocritical behavior observed in the damping measurements.

which shows K_1 to be independent of temperature, with a value ($K_1 \simeq 6\times10^{-7}$ dyn) close to that reported in literature ($K_1=6.8\times10^{-7}$ dyn for 8OCB [26], $K_1=9.3\times10^{-7}$ dyn for TBBA [11]). This value of K_1 suggests again that anharmonic effects are compatible with the first-order development of the theory. This point could be tested by direct measurements of K_1. It should be noted that, owing to the disappearance of high-frequency measurements as a result of the substantial increase in ultrasound damping, it was not possible to determine ratio B/C and K_1 for temperatures below $T_C^*+4\,°\mathrm{C}$.

2. Analysis of the critical effects

We shall first analyze the results obtained for $\theta=90°$, this being the orientation for which the critical effects are the most marked.

a. Analysis of the measurements for $\theta=90°$. Figure 9 shows the behavior of α/f^2 obtained after subtracting the anharmonic effects. The fact that α/f^2 is independent of frequency indicates that the data correspond to the hydrodynamic regime. The anharmonic effects having been subtracted, Eq. (37) is reduced to the following expression:

$$\left(\frac{\alpha(90°)}{f^2}\right)=Q(T-T_C^*)^{-x}+a(90°), \tag{38}$$

which will be used for analysis of our results.

In order to reduce the number of adjustable parameters, we imposed the value of T_C^* deduced from the analysis of the velocity measurements, since the damping and velocity measurements have been taken simultaneously. In these conditions, Eq. (38) only contains three adjustable parameters: Q, x, and $a(90°)$. Figure 9 shows that the measurements are well represented by Eq. (38). The fit of the theoretical curve to the experimental data is shown as solid line, and corresponds to the following parameters:

$$Q=[33.7\pm1]\times10^{-14}\ \mathrm{s^2\,cm^{-1}\,K^{-1}},$$

$$x=1.58\pm0.04,$$

$$a(90°)=[175\pm25]\times10^{-17}\ \mathrm{s^2\,cm^{-1}}.$$

The exponent $z\nu$ deduced from exponents $\bar{\alpha}$ and x ($x=\bar{\alpha}+z\nu$) is of the order of one, which corresponds to conventional critical slowing down. The value of the critical acoustic relaxation time τ_0 ($q=0$) can be deduced from Eq. (30) using the critical parameters determined from the analysis of the damping and velocity measurements. The value so obtained leads to a relaxation frequency of the order of 2 MHz for $T-T_C^*=3\,°\mathrm{C}$. This seems to indicate that the result at 9 MHz should correspond to the high-frequency regime, whereas it is clear from Fig. 9 that they correspond to the hydrodynamic regime. This difference shows that the Andereck and Swift theory does not fully apply to the Sm-A–Hex-B transition, since it gives incorrect critical-effect amplitudes [the P and Q coefficients of Eqs. (25) and (26)].

Figure 10 compares the critical part of the damping to the anharmonic contribution calculated at 9 MHz using elastic constants A, B, and C deduced from the velocity measurements and the value of K_1 (6×10^{-7} dyn) as determined above. This comparison indicates that near the transition the amplitude of the critical effects becomes greater than that of the anharmonic effects, unlike the case of $\theta=0°$, as will be seen below.

b. Analysis of the measurements for $\theta=0°$. Figure 11 shows the behavior of α/f^2 obtained after subtracting the anharmonic effects. The fact that α/f^2 is practically independent of temperature for $T>T_C^*+10\,°\mathrm{C}$ indicates that the critical effects are negligible in this temperature range. The value of α/f^2 ($\alpha/f^2=1300\times10^{-17}\ \mathrm{sec^2\,cm^{-1}}$) therefore represents the value of the background-damping term $a(0°)$.

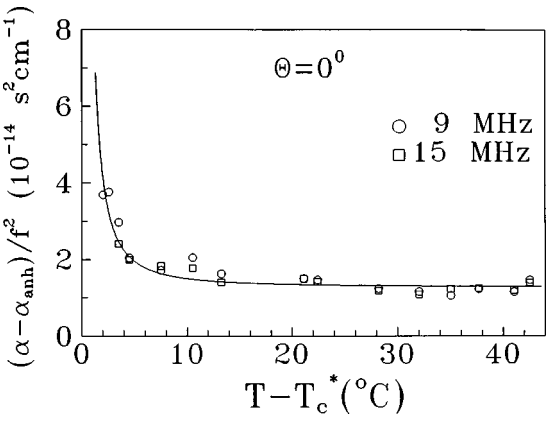

FIG. 11. Behavior of α/f^2 obtained for $\theta=0°$ after subtracting the anharmonic effects. The fact that α/f^2 is frequency independent indicates that the measurements are in the hydrodynamic regime. In contrast to the result obtained for $\theta=90°$, the critical effects are negligible in the temperature range studied. The solid line is calculated from Eq. (39) and the parameters are deduced from the analysis of velocity and $\theta=90°$-damping measurements.

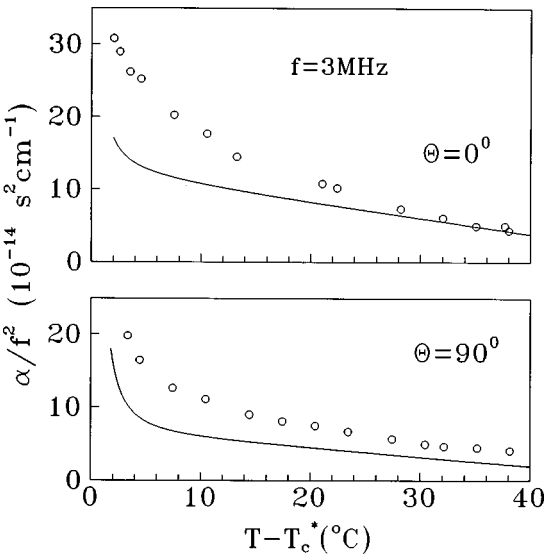

FIG. 12. Comparison of the 3-MHz damping measurements (the dots) and the damping calculated from Eq. (37) (the solid lines) using the parameters resulting from the fits at 9, 15, and 21 MHz. Possible explanations for the discrepancies between the experimental data and the calculated curves are given in the text.

This value is greater than that obtained for $\theta=90°$, as expected from the MPP theory, and presents the same order of magnitude as that measured in TBBA.

The anharmonic effects having been subtracted, Eq. (37) is reduced to the following expression:

$$\left(\frac{\alpha(0°)}{f^2}\right)=Q\left(1-\frac{\gamma_u}{\gamma_\rho}\right)^2(T-T_C^*)^{-x}+a(0°). \qquad (39)$$

This equation enables us to calculate $\alpha(0°)/f^2$, since all the parameters are known, and their values are as follows:

$$T_C^*=T_{N\text{-}I}-55.1\ °\text{C},$$

$$\gamma_u/\gamma_\rho=0.49,$$

$$x=1.58,$$

$$Q=33.7\times10^{-14}\ \text{s}^2\,\text{cm}^{-1}\,\text{K}^{-1}.$$

The first two parameters are deduced from analysis of the velocity measurements, the last two from that of the damping measurements for $\theta=90°$. The result obtained is shown as a solid line in Fig. 11. The agreement between this curve and the experimental data shows that all the analyses carried out on damping and velocity are compatible with each other.

As for $\theta=90°$, we have compared the critical part of the damping to the anharmonic contribution calculated at 9 MHz. This comparison, made in Fig. 10, shows that the anharmonic contribution is always higher than the critical contribution, which explains the pseudocritical behavior observed for this orientation.

Since our results can be globally interpreted by the fluctuation theory proposed by Andereck and Swift [16] for the Sm-A–Sm-C transition and transposed to the present case, it is therefore probable that the relaxation effects proposed by Pleiner and Brand [27] are weak. One essential feature that differentiates the fluctuation theory from the theory of Pleiner and Brand concerns high-frequency damping behavior, since the contribution of relaxation indicates that damping is independent of frequency in the $\omega\tau\gg1$ regime, whereas the contribution of fluctuations predicts that it should vary as $f^{1+\bar{\alpha}/z\nu}$ [16]. Therefore, a decisive test could consist in studying the $\omega\tau\gg1$ regime which appears near the transition temperature. This study is unfortunately not feasible in the present case, owing to the very high damping. It should be noted that Liu [28] envisaged a similar relaxation mechanism in the high-temperature phase of the N-SmA transition, and experimental study of this transition [29] showed that this mechanism was totally masked by the contribution of fluctuation effects.

B. Analysis of the 3-MHz results

We now consider the 3-MHz measurements for $\theta=0°$ and 90°, which are shown in Fig. 12. The solid lines in this figure represent, for each orientation, the damping calculated from the parameters determined at 9, 15, and 21 MHz. A substantial discrepancy can be seen between the experimental results and those calculated, for which various possible explanations exist.

The first consists in assuming the existence of defects in the sample, which could increase low-frequency damping. The second could reside in the fact that the transition takes place in a system of strongly fluctuating layers. This being the case, we can suppose that a coupling exists between the critical effects and the anharmonic effects, which is the results of the frustration associated with the layer curvature mentioned by Selinger [12]. This coupling would be more effective at low frequency than at high frequency, since anharmonic effects increase as frequency decreases. This

would explain why our analysis only gives coherent results at high frequencies.

CONCLUSION

This study should be considered as an attempt to understand the dynamics of the Sm-A–Hex-B transition using ultrasound techniques.

The results obtained show that velocity and damping of the ultrasound waves present, in the Sm-A phase, very anisotropic critical effects, which are more marked for a wave traveling in the plane of the smectic layers ($\theta=90°$) than for one traveling perpendicularly to these layers ($\theta=0°$). This anisotropy is reasonably well explained by the theory elaborated by Andereck and Swift [16] for the Sm-A–Sm-C transition, and transposed to the Sm-A–Hex-B transition. This theory is based on the existence of terms that couple the order parameter to density variation on the one hand ($[\delta\rho]\psi^2$ coupling), and to the layer-spacing gradient on the other ($[\nabla_z u]\psi^2$ coupling).

Analysis of the velocity data shows that the anisotropy rate, characterized by the γ_u/γ_ρ ratio, is of the order of 0.5, which indicates critical effects approximately four times greater in the direction parallel to the layers than in the perpendicular direction. The same analysis gives a value of the specific-heat exponent $\bar{\alpha}$ of the order of 0.6. This value, which is far from that associated with the 3D-XY universality class -0.007 to which this transition should, in principle, belong, confirms the results obtained by calorimetry. The existence of important layer fluctuations, revealed by the anharmonic effects, could explain the unusually high value of the exponent. It should be noted that this value may also reflect a 2D→3D change of regime associated with Gaussian precritical fluctuations, as has been pointed out by Brock *et al.* [9].

The damping measurements were analyzed assuming damping to be the sum of three effects: a critical effect, an anharmonic effect, and a conventional viscosity effect. The critical effect is the dominant one when wave propagation is parallel to the smectic layers. On the other hand, the anharmonic effect is preponderant when propagation is perpendicular to the layers, and its importance, which stems from the fact that the layer-rigidity modulus B is very high for this compound, explains the apparent pseudocritical behavior observed for this propagation. Analysis of these measurements indicates that the dynamical exponent $z\nu$ is of the order of one, which corresponds to conventional critical slowing down.

If the damping measurements obtained at 9, 15, and 21 MHz can be explained by our analysis, those obtained at 3 MHz cannot. This difference could come either from experimental problems (the existence of defects which might increase low-frequency damping) or from a frustration of the hexatic order due to the curvature of the smectic layers. This frustration could lead to a coupling between the critical and anharmonic effects, whereas these effects have been assumed to be uncoupled.

An interesting development of this study would be to investigate a compound with a quasi-second-order Sm-A–Hex-B phase transition and a smaller critical relaxation frequency, which would enable us to characterize the behavior near T_c (i.e. the $\omega\tau\gg 1$ regime). It would also be interesting to study a compound that does not present anharmonic effects at ultrasonic frequencies.

[1] J. M. Kosterlitz and D. J. Thouless, J. Phys. C **6**, 1181 (1973).
[2] B. I. Halperin and D. R. Nelson, Phys. Rev. Lett. **41**, 121 (1978); D. R. Nelson and B. I. Halperin, Phys. Rev. B **19**, 2456 (1979); **21**, 5312 (1980).
[3] R. J. Birgeneau and J. D. Litster, J. Phys. (France) Lett. **39**, 399 (1978).
[4] See, for example, R. Pindak, D. E. Moncton, S. C. Davey, and J. W. Goodby, Phys. Rev. Lett. **46**, 1135 (1981).
[5] See, for example, the following recent reviews: C. C. Huang and T. Stoebe, Adv. Phys. **42**, 343 (1993); J. Thoen, Int. J. Mod. Phys. B **9**, 2157 (1995).
[6] R. Bruinsma and G. Aeppli, Phys. Rev. Lett. **48**, 1625 (1982).
[7] A. Aharony, R. J. Birgeneau, J. D. Brock, and J. D. Litster, Phys. Rev. Lett. **57**, 1012 (1986).
[8] C. C. Huang, G. Nounesis, R. Geer, J. W. Goodby, and D. Guillon, Phys. Rev. A **39**, 3741 (1989); G. Nounesis, R. Geer, H. Y. Liu, C. C. Huang, and J. W. Goodby, *ibid.* **40**, 5468 (1989).
[9] J. D. Brock, D. Y. Noh, B. R. McClain, J. D. Litster, R. J. Birgeneau, A. Aharony, P. M. Horn, and J. C. Liang, Z. Phys. B **74**, 197 (1989).
[10] H. Haga, Z. Kutnjak, G. S. Iannacchione, S. Quian, D. Finotello, and C. W. Garland, Phys. Rev. E **56**, 1808 (1997).
[11] D. Collin, J. L. Gallani, and P. Martinoty, Phys. Rev. A **34**, 2255 (1986), and references cited therein.
[12] J. V. Selinger, J. Phys. (France) **49**, 1387 (1988).
[13] J. L. Gallani, P. Martinoty, D. Guillon, and G. Poeti, Phys. Rev. A **37**, 3638 (1988).
[14] P. C. Martin, O. Parodi, and P. S. Pershan, Phys. Rev. A **6**, 2401 (1972).
[15] G. F. Mazenko, S. Ramaswamy, and J. Toner, Phys. Rev. Lett. **49**, 51 (1982); Phys. Rev. A **28**, 1618 (1983).
[16] B. S. Andereck and J. Swift, Phys. Rev. A **25**, 1084 (1982).
[17] J. W. Goodby, Mol. Cryst. Liq. Cryst. Lett. **72**, 95 (1981).
[18] G. Albertini, S. Melone, G. Poeti, F. Rustichelli, and G. Torquati, Mol. Cryst. Liq. Cryst. **104**, 121 (1984).
[19] G. Poeti, E. Fanelli, and D. Guillon, Mol. Cryst. Liq. Cryst. Lett. **82**, 107 (1982).
[20] See, for example, Y. Thiriet and P. Martinoty, J. Phys. (France) **40**, 789 (1979); D. Rogez, J. L. Gallani, and P. Martinoty, Phys. Rev. Lett. **80**, 1258 (1998).
[21] D. Guillon (private communication).
[22] See, for example, K. J. Stine and C. W. Garland, Phys. Rev. A **39**, 3148 (1989); G. Nounesis, C. W. Garland, and R. Shashidar, *ibid.* **43**, 1849 (1991).
[23] The correction-to-scaling exponent is not known for this transition.
[24] C. C. Huang, C. Nounesis, and D. Guillon, Phys. Rev. A **33**, 2602 (1986).

[25] D. Collin, J. L. Gallani, and P. Martinoty, Phys. Rev. Lett. **61**, 102 (1988).
[26] J. Als-Nielsen, J. D. Litster, R. J. Birgeneau, M. Kaplan, C. R. Safinya, A. Lindegaard-Andersen, and S. Mathiesen, Phys. Rev. B **22**, 312 (1980).
[27] H. Pleiner and H. R. Brand, Phys. Rev. A **39**, 1563 (1989).
[28] M. Liu, Phys. Rev. A **19**, 2090 (1979).
[29] P. Sonntag, D. Collin, and P. Martinoty (unpublished).